

ABUNDANCES OF METAL-RICH H II REGIONS IN M51¹

FABIO BRESOLIN

Institute for Astronomy, 2680 Woodlawn Drive, Honolulu, HI 96822; *bresolin@ifa.hawaii.edu*

DONALD R. GARNETT

Steward Observatory, University of Arizona, 933 N. Cherry Ave., Tucson, AZ 85721; *dgarnett@as.arizona.edu*

AND

ROBERT C. KENNICUTT, JR.

Steward Observatory, University of Arizona, 933 N. Cherry Ave., Tucson, AZ 85721; *robk@as.arizona.edu*

ABSTRACT

We have obtained multi-object spectroscopy of H II regions in the spiral galaxy M51 with the Keck I telescope and the Low Resolution Imaging Spectrometer. For ten objects we have detected the auroral line [N II] λ 5755, while [S III] λ 6312 has been measured in seven of these. This has allowed us to measure the electron temperature of the gas and to derive oxygen, sulfur and nitrogen abundances for the ten H II regions. Contrary to the expectations from previous photoionization models of a few H II regions in M51 and from strong-line abundance indicators, the O/H abundance is below the solar value for most objects, with the most metal-rich H II regions, P 203 and CCM 72, having $\log(\text{O}/\text{H}) = -3.16$ [$\sim 1.4 (\text{O}/\text{H})_{\odot}$] and $\log(\text{O}/\text{H}) = -3.29$ [$\sim 1.0 (\text{O}/\text{H})_{\odot}$], respectively. The reduction of O/H by factors up to two or three with respect to previous *indirect* determinations has important consequences for the calibration of empirical abundance indicators, such as R_{23} , in the abundance and excitation range found in the central regions of spiral galaxies. The abundance gradients in these galaxies can therefore be considerably flatter than those determined by making use of such empirical calibrations. The H II regions with a measured electron temperature span the 0.19–1.04 R_0 range in galactocentric radius, and indicate a shallow abundance gradient for M51: $-0.02 \pm 0.01 \text{ dex kpc}^{-1}$. The S/O abundance ratio is found to be similar to previous determinations of its value in other spiral galaxies, $\log(\text{S}/\text{O}) \approx -1.6$. Therefore, we find no evidence for a variation in massive star initial mass function or nucleosynthesis at high oxygen abundance. An overabundance of nitrogen is measured, with $\log(\text{N}/\text{O}) \simeq -0.6$. Based on our new abundances we revise the effective yield for M51, now found to be almost four times lower than previous estimates, and we discuss this result within the context of chemical evolution in galactic disks. Features from Wolf-Rayet stars (the blue bump at 4660 Å and the C III line at 5696 Å) are detected in a large number of H II regions in M51, with the C III λ 5696 line found preferentially in the central, most metal-rich objects.

Subject headings: galaxies: abundances — galaxies: ISM — galaxies: spiral — galaxies: individual (NGC 5194) — H II regions

1. INTRODUCTION

Measuring the chemical abundances of gaseous nebulae is a crucial step to understand the chemical evolution and the nucleosynthesis in spiral galaxies. Historically, one of the main obstacles has been the unavailability of electron temperatures (T_e) at high metallicity. This is due to the enhanced cooling via far-IR lines causing the faint auroral lines that are necessary to determine T_e (e.g. [O III] λ 4363, [N II] λ 5755, [S III] λ 6312) to drop below detectability in the spectra of H II regions. This difficulty affects the observations of nebulae lying in the inner portions of most spiral galaxies, where the oxygen abundance can exceed the solar value [$\log(\text{O}/\text{H})_{\odot} = -3.31$, Allende Prieto, Lambert & Asplund 2001]. In order to make this important astrophysical problem tractable, strong-line methods have been calibrated and almost universally adopted for the study of abundance gradients in spirals and, more recently, to estimate chemical abundances in high-redshift star-forming galaxies (Alloin et al. 1979;

Pagel et al. 1979; Edmunds & Pagel 1984; Dopita & Evans 1986; McGaugh 1991; Díaz & Pérez-Montero 2000; Pilyugin 2000; Kewley & Dopita 2002; Denicoló et al. 2002; Kobulnicky, Henry & Phillips 2003; Pettini & Pagel 2004). While these methods can be calibrated empirically at low metallicity, nebular photoionization models have provided the necessary calibration at high metallicity (around the solar value and above), because of the lack of reliable H II region abundances.

From the observations of a few extragalactic H II regions that were believed to be extremely metal-rich (Kinkel & Rosa 1994; Díaz et al. 2000; Castellanos, Díaz & Terlevich 2002; Kennicutt, Bresolin & Garnett 2003) a disconcerting discrepancy emerges between T_e -based oxygen abundances and those derived through indirect means, the former being smaller by factors of a few. These results suggest that the oxygen abundance in the inner disks of spiral galaxies barely exceeds the solar value, while strong-line methods would suggest abundances 2–3 times higher.

It is clear that this is exploration ground for large aperture telescopes, given the faintness of the auroral lines one needs to measure in order to obtain electron temperatures at high metallicity. A first step in this direction has been taken by Garnett, Kennicutt & Bresolin (2004), who used the 6.5m MMT

¹ The data presented herein were obtained at the W.M. Keck Observatory, which is operated as a scientific partnership among the California Institute of Technology, the University of California and the National Aeronautics and Space Administration. The Observatory was made possible by the generous financial support of the W.M. Keck Foundation

telescope on Mt. Hopkins, Arizona, to obtain electron temperatures from the [N II] $\lambda 5755$ line for two H II regions in M51, CCM 10 and CCM 72. The H II regions in this galaxy have long been considered to be extremely metal-rich, based on their very low excitation (weak [O III] $\lambda \lambda 4959, 5007$ lines relative to $H\beta$) and on the results of photoionization models by Díaz et al. (1991). The metallicity obtained by Garnett et al. (2004), however, is roughly a factor of three smaller, barely exceeding the solar O/H value in the most metal-rich object, CCM 72.

In this paper we present an enlarged sample of H II regions in M51, observed with the Keck I telescope. The deeper spectra we obtained allowed us to measure the [N II] $\lambda 5755$ line in ten H II regions, in conjunction with [S III] $\lambda 6312$ in seven of them. The larger number of objects and the measurement of two auroral lines increases our confidence about the conclusions drawn in the previous work. These observations, together with the data reduction, are described in § 2. The determination of electron temperatures and chemical abundances is presented in § 3. Major results on the oxygen, nitrogen and sulfur abundances can be found in § 4. The impact of the resulting abundances on the calibration of strong-line methods is discussed in § 5. The Wolf-Rayet (WR) features detected among these H II regions are briefly presented in § 6. A few considerations on effective yields and the gas fractions in M51 are addressed in § 7, and we summarize our conclusions in § 8.

2. OBSERVATIONS

Spectroscopic observations of H II regions in M51 were carried out on the night of April 24, 2003 at the W. M. Keck Observatory on Mauna Kea, with the Keck I telescope equipped with the Low Resolution Imaging Spectrometer (Oke et al. 1995). The night was photometric, with seeing at or below $1''$. Using the blue and red channels of the spectrograph with a dichroic beam splitter, we obtained simultaneous observations at wavelengths below and above $\sim 5300 \text{ \AA}$. For the blue setting a $600 \text{ lines mm}^{-1}$ grism blazed at 4000 \AA was used, providing spectra with a resolution of 4 \AA FWHM on a mosaic of two $2K \times 4K$ Marconi CCDs down to the UV atmospheric cutoff. For the red spectra the main observations, covering roughly the $5300\text{--}7200 \text{ \AA}$ wavelength range, were carried out with a $900 \text{ lines mm}^{-1}$ grating blazed at 5500 \AA (3.5 \AA resolution) and a $2K \times 2K$ SITE CCD. Additional spectra with a $400 \text{ lines mm}^{-1}$ grating blazed at 8900 \AA (7 \AA resolution, $7000\text{--}10,000 \text{ \AA}$ approximate coverage) were obtained for the measurement of the near-IR sulfur lines at $\lambda \lambda 9069, 9532 \text{ \AA}$. However, due to the limited near-IR extension of the calibration data, only the $\lambda 9069$ fluxes are useful, and the $\lambda 9532$ fluxes were estimated from the theoretical ratio $\lambda 9532/\lambda 9069 = 2.44$.

Two slit masks were used for the multi-object spectroscopy, containing 21 and 16 $1/2$ -wide slits, respectively, with slit lengths typically in the $10\text{--}20$ arcsec range. The slits were oriented in the North-South direction, and the airmass during the observations was below 1.3. Archival V, R and $H\alpha$ images of M51 provided the necessary astrometry for the mask preparation. The target H II regions were selected among the brightest available in M51. A finding chart is shown in Fig. 1. Five objects are in common with the previous work by Bresolin, Kennicutt & Garnett (1999): CCM 10, 53, 55, 71A and 72 (catalog numbers from Carranza, Crillon & Monnet 1969).

The observations analyzed in this paper consist of 2×1800 s exposures in each of the $600/4000$ and $900/5500$ setups for the

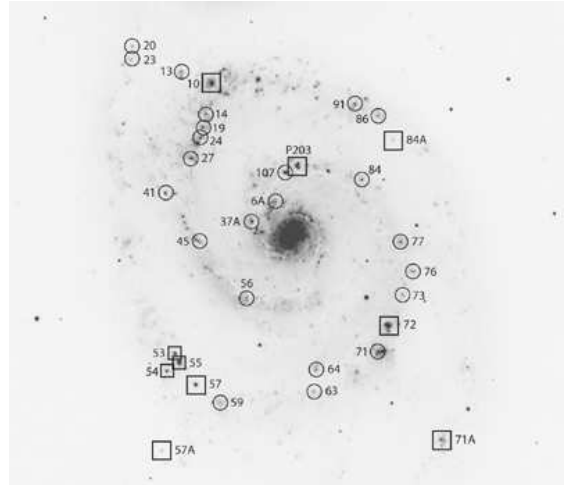


FIG. 1.— Identification of the H II regions included in the Keck multi-object observations, plotted on top of a Kitt Peak 0.9m telescope $H\alpha$ image of M51 (image courtesy T. Rector; N at top, E at left). Numbers are from Carranza, Crillon & Monnet (1969), except for P 203 (Petit et al. 1996). Squares mark the H II regions analyzed in this paper.

first mask (objects east of the galactic nucleus), and 3×1800 s in each setup for the second (west of the nucleus). Two 900 s exposures were used for the near-infrared ($400/8900$) spectra. The spectrum from each slit was treated as a separate spectrum, and reduced with common IRAF² routines. Standard star spectra obtained at the start, middle and end of the night provided the flux calibration. A standard extinction curve for Mauna Kea was adopted for the atmospheric extinction correction (Krisciunas et al. 1987).

The spectral region in common between the red and near-infrared spectra was used for flux normalization, together with the flux in the Paschen 9 and Paschen 10 lines relative to $H\beta$ when available. This procedure introduced some additional uncertainty in the [S III] $\lambda \lambda 9069, 9532$ /[S II] $\lambda 6312$ line flux ratio, from which the electron temperature in the intermediate-excitation zone is derived (see §3). Given the insufficient useful overlap between the blue and red spectra, emission line fluxes in the red spectra were adjusted relative to the fluxes in the blue spectra by scaling the flux in the $H\alpha$ line so that $H\alpha/H\beta = 3.00$ as in case B at $T_e = 6,000$ K. The ratio of the [N II] $\lambda \lambda 6548, 6583$ to [N II] $\lambda 5755$ line fluxes, from which the electron temperature in the low-excitation zone is derived, is unaffected by scaling errors, as these lines fall on the same spectra (the $900/5500$ ones). Moreover, this ratio is also largely insensitive to uncertainties in reddening given the small wavelength baseline involved.

The reddening coefficient $C(H\beta)$ was determined from the Balmer decrement using the $H\beta$, $H\gamma$ and $H\delta$ lines, adopting the case B theoretical ratios at $T_e = 6,000$ K, and the interstellar reddening law of Cardelli, Clayton & Mathis (1989). We have measured the [N II] $\lambda 5755$ auroral line in ten H II regions. Out of these objects, [S III] $\lambda 6312$ has been measured in seven cases. The IR spectrum of CCM 57A, however, fell outside of the area covered by the CCD, and therefore for this object we could not measure $T[S III]$ in the way outlined in § 3. The [O III] $\lambda 4363$ line remained undetected

² IRAF is distributed by the National Optical Astronomy Observatories, which are operated by the Association of Universities for Research in Astronomy, Inc., under cooperative agreement with the National Science Foundation.

in all objects, while [O II] λ 7325 was detected in CCM 10, CCM 57, CCM 71A and CCM 72, however with a generally poor signal-to-noise ratio. Besides the two nebulae in common with the study by Garnett et al. (2004), this is the first time that auroral lines are measured in a large number of H II regions in M51. We will concentrate the rest of our analysis on the ten objects with a measured [N II] λ 5755 line, as information on electron temperatures and chemical abundances can be obtained directly only for these H II regions. The fluxes for their most important lines, corrected for reddening and normalized to $F(\text{H}\beta)=100$, are presented in Table 1, where each H II region is identified by its CCM number. The H II region P 203, 7" West and 61" North of the M51 nucleus, not included in the Carranza et al. (1969) catalog, is identified from Petit et al. (1996). The errors quoted in the Table reflect uncertainties in the flat fielding and the flux calibration, as well as statistical errors, which dominate in the case of the fainter lines (e.g. the auroral lines). The comparison concerning line fluxes for objects in common with other authors, in particular Bresolin et al. (1999) and Garnett et al. (2004) (CCM 10 and CCM 72), is generally good. The agreement with these works is typically at the 5 percent level or better for the [N II] and [S II] lines, and at the 15 percent level or better for the [O II], [O III] and [S III] lines. A notable exception is given by the [O III] lines of CCM 53 (46 percent larger than in the Bresolin et al. 1999 paper), and the [S III] λ 9069,9532 lines of CCM 71A (a factor of two smaller). At least for the latter H II region, a well extended object with multiple emission peaks, differences in pointing can be responsible for the disagreement. Large differences are also found for CCM 10 when comparing with the line intensities reported by Díaz et al. (1991).

3. ELECTRON TEMPERATURES AND ABUNDANCES

As in our previous work on M101 (Kennicutt et al. 2003) and on the M51 H II regions CCM 72 and CCM 10 (Garnett et al. 2004), we adopt a three-zone model to describe the ionization structure of an H II region. These zones are characterized by different electron temperatures T_e , each referring to different, coexisting atomic ionization stages: [O II], [N II], [S II] in the low-ionization zone, [S III], [Ar III] in the intermediate-ionization zone, and [O III], [Ne III] in the high-ionization zone. The photoionization models of Garnett (1992) predict simple scaling relations between the temperature in the different zones, applicable in a wide $T[\text{O III}]$ range (2,000–18,000 K):

$$T[\text{S III}] = 0.83 T[\text{O III}] + 1700 \text{ K}, \quad (1)$$

$$T[\text{N II}] = T[\text{O II}] = 0.70 T[\text{O III}] + 3000 \text{ K}. \quad (2)$$

Observational evidence in support of these relationships, in particular Eq. (1), has been provided by a few authors (e.g. Garnett et al. 1997; Kennicutt et al. 2003). One could consider alternative formulations, for example the relationship between $T[\text{O II}]$ and $T[\text{O III}]$ given by Izotov et al. (1994), based on the grid of photoionization models by Stasinska (1990). For the same measured value of $T[\text{O II}]$, their Eq. (4) would lead to $T[\text{O III}]$ lower by a few hundred degrees relative to the Garnett (1992) equation. However, if we limit the Stasinska models to $T_{\text{eff}} < 40,000$ K for the ionizing stars,

as seems appropriate for the H II regions in M51, we obtain good agreement between the two different sets of photoionization models.

We established from the [S II] λ 6717/[S II] λ 6731 line ratio that all the H II regions are in the low-density regime ($N_e < 150 \text{ cm}^{-3}$). Subsequently, using the five-level atom program *nebular* implemented in IRAF/STSDAS (Shaw & Dufour 1995), we determined the electron temperatures $T[\text{N II}]$ (ten objects) and $T[\text{S III}]$ (six objects) from the emission line ratios [N II] λ 6548,6583/[N II] λ 5755 and [S III] λ 9069,9532/[S III] λ 6312, respectively. The results are summarized in Table 2. As in the M101 Kennicutt et al. (2003) paper, we have updated the S III collisional strengths used by *nebular* adopting the results by Tayal & Gupta (1999).

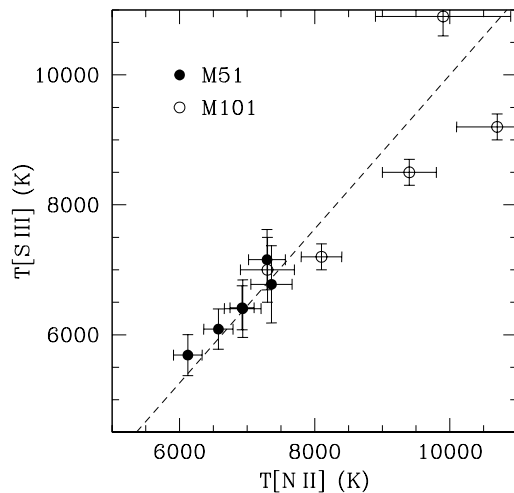


FIG. 2.— Relationship between $T[\text{N II}]$ and $T[\text{S III}]$ measured for H II regions in M51 (this work: full dots) and M101 (Kennicutt et al. 2003: open dots). The model prediction from Garnett (1992) is drawn as a dashed line.

A good agreement is found with the independent $T[\text{N II}]$ determinations by Garnett et al. (2004) for CCM 10 (+1000,-600 K) and for CCM 72 (6000 ± 300 K). To verify the H II region zone model adopted for the following analysis, we have considered the correlation between $T[\text{N II}]$ and $T[\text{S III}]$ for the six M51 objects where both temperatures are available. As Fig. 2 shows, the observed relation agrees very well with the expectations based on the Garnett (1992) models (dashed line). This result is encouraging, since it lends support to the H II region zone model adopted here, indicating that the electron temperatures in the different excitation zones can be well established even when only one auroral line (e.g. [N II] λ 5755 at low excitation) is available. We have therefore calculated the 'missing' temperature for the high-ionization zone $T[\text{O III}]$, using both equations (1) and (2), and taking a weighted average for the result when both $T[\text{N II}]$ and $T[\text{S III}]$ are available. This gives us electron temperature estimates for the high-, intermediate- and low-ionization zones as described above; the results are listed in Table 3. For six of the ten objects listed we have two independent estimates of $T[\text{O III}]$, which we have averaged, from our measured $T[\text{N II}]$ and $T[\text{S III}]$. We note that the 2σ value of $T[\text{S III}] \approx 5400$ K for CCM 72 from Garnett et al. (2004) is very close to our result (5700 ± 300 K). The lowest temperature in our H II re-

TABLE 1
 DEREDDENED LINE FLUXES AND ERRORS

Line	CCM 10	CCM 53	CCM 54	CCM 55	CCM 57	CCM 57A	CCM 71A	CCM 72	CCM 84A	P 203
[O II] 3727	126 ± 9	129 ± 9	115 ± 8	78 ± 5	114 ± 8	104 ± 7	147 ± 10	63 ± 6	125 ± 12	32 ± 2
[Ne III] 3869	0.7 ± 0.1	0.6 ± 0.1	1.1 ± 0.2	0.8 ± 0.1	...	12.8 ± 0.9	2.2 ± 0.2	0.4 ± 0.1	1.6 ± 0.4	...
Hδ 4101	25 ± 2	24 ± 2	24 ± 2	23 ± 1	24 ± 2	24 ± 2	25 ± 2	25 ± 2	21 ± 2	21 ± 1
Hγ 4340	48 ± 3	49 ± 3	46 ± 3	46 ± 3	47 ± 3	48 ± 3	46 ± 3	47 ± 3	45 ± 3	43 ± 3
He I 4471	2.4 ± 0.2	2.9 ± 0.2	2.4 ± 0.3	2.1 ± 0.1	2.9 ± 0.2	5.6 ± 0.4	2.7 ± 0.2	2.1 ± 0.2	4.8 ± 0.5	...
[O III] 4959	4.4 ± 0.3	11.8 ± 0.7	14.2 ± 0.9	6.7 ± 0.4	5.7 ± 0.3	60.0 ± 3.5	16.1 ± 1.0	2.4 ± 0.1	29.8 ± 1.8	1.7 ± 0.2
[O III] 5007	12.1 ± 0.7	33.3 ± 2.0	41.5 ± 2.4	19.0 ± 1.1	15.9 ± 0.9	168.6 ± 9.9	46.1 ± 2.7	6.6 ± 0.4	84.9 ± 5.1	4.9 ± 0.3
[N II] 5755	.50 ± 0.04	.54 ± 0.07	.65 ± 0.07	.43 ± 0.04	.68 ± 0.09	.48 ± 0.08	.79 ± 0.07	.28 ± 0.04	.92 ± 0.15	.15 ± 0.02
He I 5876	7.7 ± 0.5	9.4 ± 0.6	10.0 ± 0.6	8.4 ± 0.5	10.1 ± 0.6	11.4 ± 0.7	9.3 ± 0.6	5.6 ± 0.4	13.1 ± 1.0	4.5 ± 0.3
[S III] 6312	.30 ± 0.03	.31 ± 0.06	.44 ± 0.06	.31 ± 0.03	.31 ± 0.07	.62 ± 0.0916 ± 0.03
[N II] 6548	37 ± 3	40 ± 3	40 ± 3	38 ± 3	40 ± 3	23 ± 2	39 ± 3	33 ± 3	49 ± 4	26 ± 2
Hα 6563	300 ± 20	300 ± 20	300 ± 20	300 ± 20	300 ± 20	300 ± 20	300 ± 20	300 ± 27	300 ± 27	300 ± 20
[N II] 6583	112 ± 8	120 ± 8	122 ± 8	117 ± 8	124 ± 8	70 ± 5	116 ± 8	100 ± 9	144 ± 13	79 ± 5
He I 6678	2.0 ± 0.1	2.4 ± 0.2	2.6 ± 0.2	2.1 ± 0.1	2.3 ± 0.2	3.5 ± 0.3	2.7 ± 0.2	1.8 ± 0.2	3.1 ± 0.3	1.1 ± 0.1
[S II] 6717	27 ± 2	24 ± 2	36 ± 3	23 ± 2	26 ± 2	20 ± 1	41 ± 3	26 ± 2	19 ± 2	23 ± 2
[S II] 6731	19 ± 1	17 ± 1	27 ± 2	18 ± 1	19 ± 1	14 ± 1	28 ± 2	20 ± 2	15 ± 1	18 ± 1
[Ar III] 7135	2.2 ± 0.2	2.7 ± 0.3	3.6 ± 0.4	2.6 ± 0.3	2.6 ± 0.3	...	3.9 ± 0.5	1.4 ± 0.2	8.8 ± 2.8	1.7 ± 0.2
[S III] 9069	17 ± 3	18 ± 4	17 ± 3	21 ± 4	14 ± 3	...	13 ± 3	14 ± 3	17 ± 3	9 ± 2
C(Hβ)	0.25 ± 0.05	0.10 ± 0.05	0.15 ± 0.05	0.05 ± 0.05	0.15 ± 0.05	0.05 ± 0.05	0.25 ± 0.05	0.35 ± 0.10	0.60 ± 0.10	0.21 ± 0.05
EW(Hβ) (Å)	51	92	144	74	155	300	96	61	203	47

 TABLE 2
 MEASURED ELECTRON
 TEMPERATURES (K)

ID	T[N II] (K)	T[S III] (K)
CCM 10	6900 ± 200	6400 ± 300
CCM 53	6900 ± 300	6400 ± 400
CCM 54	7300 ± 300	7200 ± 500
CCM 55	6600 ± 200	6100 ± 300
CCM 57	7400 ± 300	6800 ± 600
CCM 57A	7900 ± 400	...
CCM 71A	7700 ± 200	...
CCM 72	6100 ± 200	5700 ± 300
CCM 84A	7700 ± 400	...
P 203	5600 ± 200	...

 TABLE 3
 ADOPTED ELECTRON TEMPERATURES (K)

ID	T(O ⁺ , N ⁺ , S ⁺) (K)	T(S ⁺² , Ar ⁺²) (K)	T(O ⁺² , Ne ⁺²) (K)
CCM 10	6900 ± 200	6400 ± 200	5600 ± 200
CCM 53	6900 ± 300	6400 ± 300	5600 ± 300
CCM 54	7300 ± 300	7200 ± 300	6300 ± 300
CCM 55	6600 ± 200	6100 ± 200	5200 ± 200
CCM 57	7400 ± 300	6800 ± 300	6200 ± 400
CCM 57A	7900 ± 400	7500 ± 400	7000 ± 600
CCM 71A	7700 ± 200	7300 ± 200	6800 ± 400
CCM 72	6100 ± 200	5700 ± 200	4600 ± 200
CCM 84A	7700 ± 400	7300 ± 400	6900 ± 600
P 203	5600 ± 200	4800 ± 200	3700 ± 300

gion sample is measured for P 203, close to the galactic center, which, at T[N II] = 5600 K, is the coolest extragalactic nebula to date where a direct electron temperature exists.

The ionic and element abundances derived from the electron temperatures in Table 3 using the five-level atom program are listed in Table 4 and 5, respectively. The associated errors derive mostly from the uncertainty in the electron temperatures. The uncertainty in the sulfur abundance is largest for CCM 57A, where we had to rely on $\lambda 6312$ alone for the S⁺² ionic abundance, due to the lack of the IR spectrum mentioned in § 2.

Ionization correction factors for sulfur are expected to be small in low-ionization nebulae, as is the case here. This is verified in the top panel of Fig. 3, where the ion ratio (S⁺ + S⁺²)/(O⁺ + O⁺²) is plotted against the oxygen ionization fraction O⁺/O. The M51 data are in general agreement with the trend observed for H II regions in M101 and NGC 2403 (open circles and squares, respectively), extended to higher O⁺/O, even if a couple of objects (CCM 55 and 57) display a slight offset from the average relation. The dashed line in Fig. 3 reproduces the sulfur ionization correction formula (Stasinska 1978; French 1981):

$$\frac{S^+ + S^{+2}}{S} = \left[1 - \left(1 - \frac{O^+}{O} \right)^\alpha \right]^{1/\alpha}, \quad (3)$$

where we have used $\alpha = 2.5$ and $\log(S/O) = -1.6$, which are the parameters we adopted in our M101 paper. Our new observations in M51 do not justify a change in the parameters that appear in the ionization correction formula.

In the case of argon the situation appears more complex. Unlike sulfur, only one ionization stage (Ar⁺²) is observed for this atomic species in the optical spectra of H II regions, and in low-ionization nebulae the amount of unseen Ar⁺ can become non-negligible. In our previous work on M101, we established that Ar⁺²/S⁺² is a good tracer of Ar/S, based on the near independence of this ratio on the oxygen ionization fraction (at the same time we showed that Ar⁺²/O⁺² is a bad tracer of Ar/O, and that neon has similar problems). The bottom plot of Fig. 3 suggests, however, that at high O⁺/O (low ionization) Ar⁺²/S⁺² deviates from the roughly constant

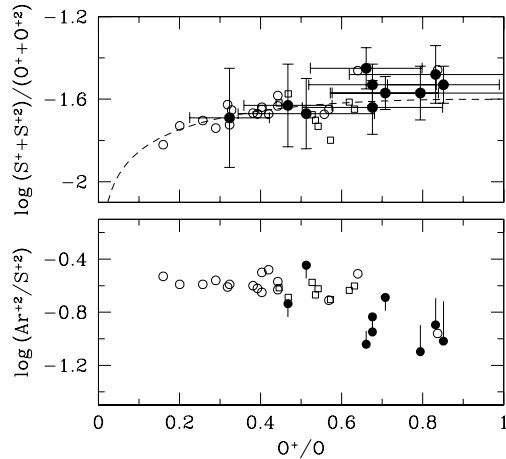


FIG. 3.— *Top*: The ion ratio $(S^+ + S^{+2})/(O^+ + O^{+2})$ plotted against the oxygen fractional ionization O^+/O for our sample of objects in M51 (full dots with error bars), and for objects studied in M101 (Kennicutt et al. 2003, open circles) and in NGC 2403 (Garnett et al. 1997, open squares). Equation (3) for the sulfur ionization correction factor provides the dashed curve. *Bottom*: Ar^{+2}/S^{+2} plotted against O^+/O for the same sample of objects as above. A correlation with ionization seems to occur at large O^+/O values. The vertical bars show the estimated correction factors for the M51 H II regions (see text for explanation).

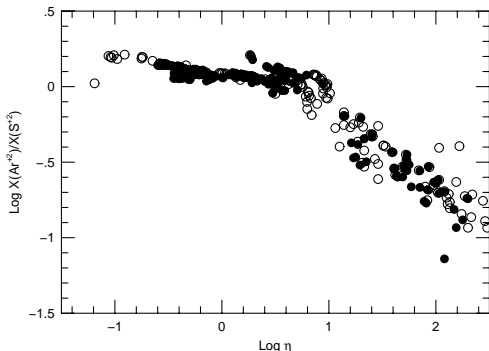


FIG. 4.— The predicted correlation between the $X(Ar^{+2})/X(S^{+2})$ ionic fraction and the radiation softness parameter η from the models of Stasinska et al. (2001). The latter are plotted for an upper limit of the initial mass function of $120 M_{\odot}$ (filled circles) and $30 M_{\odot}$ (open circles), for both extended and instantaneous bursts. The ionization correction factor used to obtain the abundance ratio Ar/S from Ar^{+2}/S^{+2} can be estimated from the reciprocal of $X(Ar^{+2})/X(S^{+2})$ in this plot.

value found at higher ionization. This is likely an effect of the increase of Ar^+ with respect to Ar^{+2} at low excitation. There is, in fact, a good correlation between Ar^{+2}/S^{+2} and the hardness of the radiation field, as measured by the parameter $\eta = (O^+/O^{+2})/(S^+/S^{+2})$ (Vílchez & Pagel 1988; see Fig. 4). The ionization correction factor necessary to estimate Ar/S from Ar^{+2}/S^{+2} was obtained from the corresponding quantities in the models of Stasinska, Schaerer & Leitherer (2001), and indicate that at low excitation the correction can amount to +0.2 to +0.3 dex. The shift for each H II region in the diagram thus determined is shown by the vertical bars in Fig. 3. This ionization correction scheme also shows that at high ex-

citation (as for most of the M101 and NGC 2403 H II regions plotted) a moderate negative correction ($\simeq -0.1$ dex) should be applied to the observed Ar^{+2}/S^{+2} ratios in order to recover the real Ar/S ratios. This will remove most of the apparent decreasing trend of Ar/S with oxygen ionization fraction suggested at first from Fig. 3.

4. RESULTS FOR OXYGEN, SULFUR AND NITROGEN

The somewhat surprising result we obtain concerns the typical oxygen abundance of the M51 H II regions studied here: for most objects O/H is below the solar value [$\log(O/H)_{\odot} = -3.31$, Allende Prieto et al. 2001], and reaches ~ 1.4 times the solar value for P 203 [$\log(O/H) = -3.16$], the most oxygen-rich H II region in our sample. This contrasts with the results of detailed photoionization models by Díaz et al. (1991), who estimated highly super-solar abundances, between $\log(O/H) = -2.9$ and $\log(O/H) = -2.6$ for their objects (CCM 10 and CCM 72 are in common with our sample), and thus confirms the findings of Garnett et al. (2004). The concept of M51 as a very metal-rich (largely over-solar) spiral galaxy, supported since the early 1990's, based on the above-mentioned models and the accepted calibrations of several empirical abundance determination methods, in particular R_{23} (Vila-Costas & Edmunds 1992), is not fully supported by our data. The results for P 203, on the other hand, suggest that the central region of the galaxy, where the excitation is very low, contains nebulae with a O/H ratio at least 40% larger than the solar value. The discussion of additional low-excitation H II regions near the M51 nucleus is deferred to the end of § 5.

Column 2 in Table 5 lists the deprojected distance from the galaxy center in units of the isophotal radius ($R_0 = 5.4$ arcmin, corresponding to 13.2 kpc if the distance of 8.4 Mpc is adopted from Feldmeier et al. 1997). Our data span the disk from $R/R_0 = 0.19$ to $R/R_0 = 1.04$, but with the majority of the objects concentrated around $R/R_0 = 0.5$. As a result the radial trends of abundances and abundance ratios depend heavily on the H II regions at the two opposite extremes of the range, P 203 (inner) and CCM 71A (outer). We plot the radial distribution of O/H , N/O and S/O in Fig. 5, which indicates a rather shallow O/H gradient in M51. The dashed line represents the linear regression to the data points:

$$12 + \log(O/H) = 8.72 (\pm 0.09) - 0.28 (\pm 0.14) R/R_0 \quad (4)$$

The gradient from equation (4) corresponds to -0.02 ± 0.01 dex kpc^{-1} . The central O/H abundance ratio suggested by the regression is about solar or slightly above solar, but we cannot exclude a steepening of the relation at small galactocentric radii. Clearly, data for additional H II regions are needed to better constrain the abundance gradient in M51. There is considerable scatter at a given radial distance, amounting to ~ 0.4 dex in O/H around $R/R_0 = 0.5$. This is not atypical, since scatter of a similar magnitude is observed in other well-studied spiral galaxies (Kennicutt et al. 2003; Garnett et al. 1997). Finally, the radial trend of both N/O and S/O are consistent with a constant value, although a very shallow N/O gradient is suggested by Fig. 5.

Plots of the abundance ratios S/O and N/O as a function of O/H are shown in Fig. 6. The S/O ratio (upper panel) for the M51 H II regions is consistent with the approximately constant value [$\log(S/O) = -1.6$] observed in other spiral galaxies, without any evidence for a decrease as the oxygen abun-

TABLE 4
 IONIC ABUNDANCES

ID	O ⁺ /H ⁺	O ²⁺ /H ⁺	N ⁺ /H ⁺	S ⁺ /H ⁺	S ²⁺ /H ⁺	Ne ²⁺ /H ⁺	Ar ²⁺ /H ⁺
CCM 10	$(3.1 \pm 0.6) \times 10^{-4}$	$(5.5 \pm 1.4) \times 10^{-5}$	$(6.8 \pm 0.7) \times 10^{-5}$	$(3.0 \pm 0.3) \times 10^{-6}$	$(7.5 \pm 1.3) \times 10^{-6}$	$(1.6 \pm 0.5) \times 10^{-5}$	$(7.2 \pm 1.5) \times 10^{-7}$
CCM 53	$(3.1 \pm 0.8) \times 10^{-4}$	$(1.5 \pm 0.6) \times 10^{-4}$	$(7.3 \pm 1.2) \times 10^{-5}$	$(2.7 \pm 0.4) \times 10^{-6}$	$(7.9 \pm 1.9) \times 10^{-6}$	$(1.5 \pm 0.7) \times 10^{-5}$	$(8.9 \pm 2.6) \times 10^{-7}$
CCM 54	$(2.1 \pm 0.5) \times 10^{-4}$	$(1.0 \pm 0.3) \times 10^{-4}$	$(6.2 \pm 0.9) \times 10^{-5}$	$(3.5 \pm 0.5) \times 10^{-6}$	$(5.6 \pm 1.1) \times 10^{-6}$	$(1.2 \pm 0.5) \times 10^{-5}$	$(8.2 \pm 2.0) \times 10^{-7}$
CCM 55	$(2.6 \pm 0.6) \times 10^{-4}$	$(1.4 \pm 0.5) \times 10^{-4}$	$(8.5 \pm 1.2) \times 10^{-5}$	$(3.3 \pm 0.4) \times 10^{-6}$	$(1.1 \pm 0.2) \times 10^{-5}$	$(3.2 \pm 1.4) \times 10^{-5}$	$(1.0 \pm 0.2) \times 10^{-6}$
CCM 57	$(2.1 \pm 0.6) \times 10^{-4}$	$(4.4 \pm 1.8) \times 10^{-5}$	$(6.1 \pm 1.0) \times 10^{-5}$	$(2.4 \pm 0.4) \times 10^{-6}$	$(5.5 \pm 1.7) \times 10^{-6}$...	$(7.0 \pm 2.6) \times 10^{-7}$
CCM 57A	$(1.2 \pm 0.4) \times 10^{-4}$	$(2.6 \pm 1.4) \times 10^{-4}$	$(2.7 \pm 0.6) \times 10^{-5}$	$(1.5 \pm 0.3) \times 10^{-6}$	$(6.2 \pm 3.0) \times 10^{-6}$	$(8.2 \pm 5.6) \times 10^{-5}$...
CCM 71A	$(2.0 \pm 0.4) \times 10^{-4}$	$(8.1 \pm 2.4) \times 10^{-5}$	$(4.8 \pm 0.6) \times 10^{-5}$	$(3.3 \pm 0.3) \times 10^{-6}$	$(4.1 \pm 0.5) \times 10^{-6}$	$(1.7 \pm 0.6) \times 10^{-5}$	$(8.4 \pm 1.1) \times 10^{-7}$
CCM 72	$(4.1 \pm 1.3) \times 10^{-4}$	$(1.0 \pm 0.4) \times 10^{-4}$	$(9.6 \pm 1.5) \times 10^{-5}$	$(4.8 \pm 0.7) \times 10^{-6}$	$(9.0 \pm 1.9) \times 10^{-6}$	$(3.8 \pm 2.2) \times 10^{-5}$	$(7.2 \pm 1.8) \times 10^{-7}$
CCM 84A	$(1.7 \pm 0.6) \times 10^{-4}$	$(1.6 \pm 1.0) \times 10^{-4}$	$(6.2 \pm 1.3) \times 10^{-5}$	$(1.6 \pm 0.3) \times 10^{-6}$	$(5.3 \pm 1.1) \times 10^{-6}$	$(1.3 \pm 1.0) \times 10^{-5}$	$(1.9 \pm 0.5) \times 10^{-6}$
P 203	$(3.2 \pm 0.8) \times 10^{-4}$	$(3.6 \pm 2.9) \times 10^{-4}$	$(1.1 \pm 0.2) \times 10^{-4}$	$(6.0 \pm 0.8) \times 10^{-6}$	$(9.8 \pm 1.7) \times 10^{-6}$...	$(1.8 \pm 0.4) \times 10^{-6}$

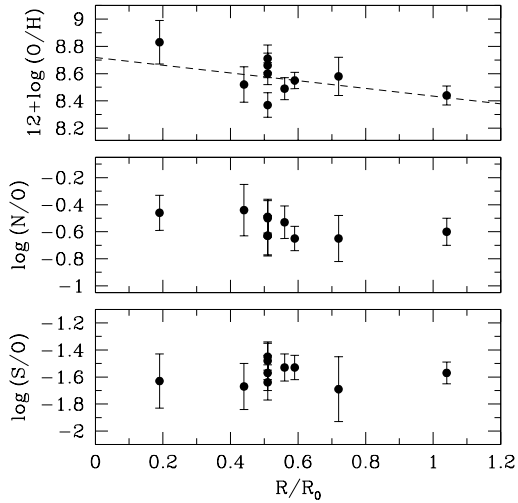

 FIG. 5.— Radial trends of $12 + \log(\text{O}/\text{H})$ (top), (b) $\log(\text{N}/\text{O})$ (middle) and $\log(\text{S}/\text{O})$ (bottom). The dashed line represents the linear fit to the O/H radial gradient (equation 4).

 TABLE 5
 TOTAL ABUNDANCES

ID	R/R_0	$12 + \log(\text{O}/\text{H})$	$\log(\text{N}/\text{O})$	$\log(\text{S}/\text{O})$
CCM 10	0.59	8.56 ± 0.07	-0.66 ± 0.10	-1.54 ± 0.09
CCM 53	0.51	8.66 ± 0.09	-0.63 ± 0.14	-1.63 ± 0.13
CCM 54	0.56	8.49 ± 0.08	-0.53 ± 0.12	-1.52 ± 0.10
CCM 55	0.51	8.60 ± 0.08	-0.49 ± 0.12	-1.44 ± 0.10
CCM 57	0.51	8.40 ± 0.09	-0.54 ± 0.14	-1.50 ± 0.14
CCM 57A	0.72	8.58 ± 0.14	-0.65 ± 0.17	-1.61 ± 0.24
CCM 71A	1.04	8.45 ± 0.07	-0.62 ± 0.10	-1.58 ± 0.08
CCM 72	0.51	8.71 ± 0.10	-0.63 ± 0.15	-1.56 ± 0.13
CCM 84A	0.44	8.52 ± 0.13	-0.44 ± 0.19	-1.64 ± 0.17
P 203	0.19	8.84 ± 0.16	-0.46 ± 0.13	-1.61 ± 0.20

dance increases. The results of Díaz et al. (1991) had provided some suggestion that such a decrease might occur (e.g. Garnett 2003). Based on our results, we therefore find no need to invoke changes in the massive star initial mass function or in the nucleosynthesis at high metallicity (at least up to approximately the solar value).

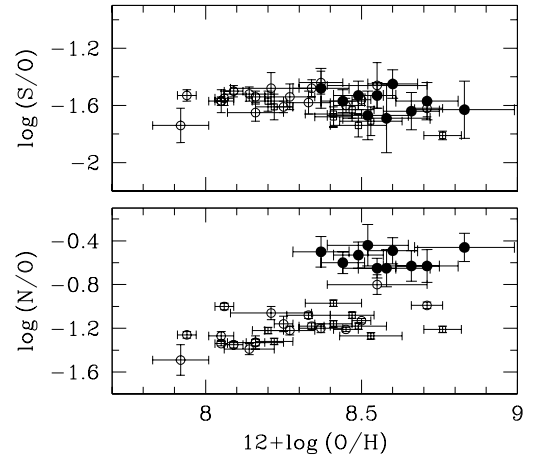


FIG. 6.— Top: The relationship between the S/O abundance ratio and O/H. Symbols are the same as in Fig. 3. A trend of approximately constant S/O is seen to extend beyond the solar oxygen abundance. Bottom: The relationship between N/O and O/H. Symbols as in Fig. 3.

The nitrogen abundance, shown in relation to O/H in the bottom panel of Fig. 6, has an average value $\log(\text{N}/\text{O}) \simeq -0.56$, higher than the value measured in H II regions of comparable oxygen abundance in galaxies like M101 and NGC 2403. This apparent nitrogen overabundance seems consistent with the known spread of N/O at a given O/H for spiral galaxies, related to differences in star formation histories, with earlier Hubble types (M51 is classified as Sbc) having on average higher N/O ratios than later types (Henry, Edmunds & Köppen 2000; Pilyugin, Thuan & Vílchez 2003).

5. EMPIRICAL ABUNDANCE INDICATORS

The results of a quarter century of research on nebular abundances have proved very useful to obtain estimates of abundance gradients in spiral galaxies and of oxygen abundances of star forming regions in the distant universe. Indirect methods (as opposed to the direct methods based on the determination of electron temperatures) using ratios of strong lines have been developed by several authors, the most widely used being arguably the R_{23} empirical abundance indicator of

Pagel et al. (1979). Some evidence has been mounting, however, against the accuracy of such methods in the abundance range typical of the central regions of spiral galaxies (half solar oxygen abundance and above). This has been discussed at length in our work on M101 (Kennicutt et al. 2003), and we will not repeat the discussion here. In that paper we also presented the main issues which could complicate the analysis based on the collisionally excited lines, namely the presence of temperature fluctuations and, at high metallicity, temperature gradients. Their effect is similar, in that the measured electron temperature is weighted towards the higher temperature zones, leading to a possible underestimate of the real nebular abundances. The reader is referred to Kennicutt et al. (2003) for further details and for a justification for the use of the collisionally excited lines. Admittedly, the issue is still open. In addition, the temperature in the [N II] zone could be overestimated from neglecting the recombination component of the $\lambda 5755$ line (see Liu et al. 2000). The lack of the line flux from [N III] at $57 \mu\text{m}$ for our M51 sample does not allow us to estimate the contribution of this recombination directly from observations. However, this contribution is likely to be small, given the small amount of N^{++} present in low-excitation nebulae. The good agreement between the observed $T[\text{N II}]-T[\text{S III}]$ relationship and the predicted one from Garnett (1992) also suggests that such a recombination component can be neglected to first order.

The detection of auroral lines in objects around the solar O/H ratio is prompting a revision of the abundances based on indirect methods, since relatively low abundances are found for objects that were once thought to be very metal-rich (i.e. well above the solar value: Castellanos et al. 2002, Kennicutt et al. 2003). This is also the case for the M51 H II regions analyzed in this work, and a brief assessment of a few representative empirical abundance indicators seems to be warranted at this point.

It is obvious that the abundances obtained in M51 in the present work have an important impact on most empirical calibrations. This is exemplified in Fig. 7, where we show the comparison of our direct oxygen abundances with those obtained by means of R_{23} , adopting two different calibrations: the one by Edmunds & Pagel (1984) and the one by Pilyugin (2001) (see Garnett et al. 2004 for a comparison involving two other calibrations). The sample of objects shown includes, besides the M51 H II regions studied here, a number of nebulae extracted from the literature (Kennicutt et al. 2003; Garnett et al. 1997; van Zee et al. 1998; Deharveng et al. 2000; Díaz & Pérez-Montero 2000; Díaz et al. 2000; Castellanos et al. 2002). We note that for the high-metallicity object CDT1 in NGC 1232 studied by Castellanos et al. (2002) we derive, using their line fluxes, an O/H value smaller by 0.13 dex than their published abundance $12 + \log(\text{O}/\text{H}) = 8.95$. Our results on the M51 H II regions clearly demonstrate the failure of the existing R_{23} calibrations at low excitation ($\log R_{23} < 0.5$), since they overestimate the abundances by 50–400 percent. This discrepancy corresponds to electron temperatures smaller by approximately 10–15 percent compared with our measured values (about 3σ to 4σ). In the particular case of CCM 72 and CCM 10, the [O II] temperatures modeled by Díaz et al. (1991) (4800 K and 6000 K, respectively) lie 4σ and 6σ below our measurements.

This result has fundamental consequences for the studies of abundance gradients in spiral galaxies based on this empirical indicator (e.g. Zaritsky et al. 1994, Vila-Costas & Edmunds 1992), and the actual gradients in the central regions will in

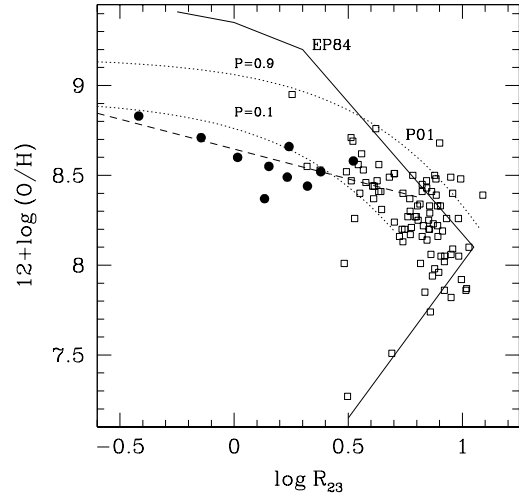


FIG. 7.— Comparison between O/H abundances obtained from measured electron temperatures (dots) and from the semi-empirical abundance indicator R_{23} (full and dotted lines). Two different R_{23} calibrations are used: Edmunds & Pagel (1984, = EP, full line) and Pilyugin (2001, = P01, dotted lines). Two curves are plotted for the latter, corresponding to two different values of the excitation parameter, $P=0.1$ and $P=0.9$. The plotted data are from the current work (full dots) and from published studies: Kennicutt et al. (2003), Garnett et al. (1997), van Zee et al. (1998), Deharveng et al. (2000), Díaz & Pérez-Montero (2000) and Castellanos et al. (2002) (open squares). The lowest excitation object, at the far left, is P203, while the most metal-rich one is CDT1 in NGC 1232 (Castellanos et al. 2002). The dashed line is a fit to the M51 points, except CCM 84A: $12 + \log(\text{O}/\text{H}) = 8.64 - 0.33 \log R_{23}$.

general be much flatter than reported in these works. The discrepancy is also not peculiar to R_{23} . As an example, Pettini & Pagel (2004) have considered an empirical abundance calibration of two line indices involving the nitrogen lines: $[\text{N II}] \lambda 6583 / \text{H}\alpha$ (see also Denicoló et al. 2002), and $([\text{O III}] \lambda 5007 / \text{H}\beta) / ([\text{N II}] \lambda 6583 / \text{H}\alpha)$. We show in Fig. 8 the position occupied in the corresponding diagrams by the M51 H II regions. A decrease in the slope at low excitation is noticed with respect to the Pettini & Pagel (2004) calibrations (shown by the dashed lines), indicating a flattening around $12 + \log(\text{O}/\text{H}) = 8.6$, which however also reflects the large nitrogen abundance found in M51 from our analysis. Fig. 9 shows instead how the O/H abundances derived through the P-method (Pilyugin 2001) compare with direct abundances. In this plot, only objects which are predicted by the P-method to have $12 + \log(\text{O}/\text{H}) > 8.2$ (the quoted range of validity for this method in the high-abundance regime) are plotted. This indicator seems to be afflicted by severe difficulties in a wide abundance range. The general conclusion we can draw is that great caution is necessary when using strong-line empirical abundance indicators for low-excitation H II regions. Erroneous results can be obtained in the inner disks of spirals up to a factor of a few.

How low can the excitation in M51 H II regions be? We report in Table 6 the line fluxes, normalized to $\text{H}\beta = 100$, measured for the H II regions belonging to the central zone of the galaxy ($R_0 = 0.12 - 0.36 R_0$) besides P203. No auroral line was detected in these objects, therefore not permitting a direct abundance determination. The total $[\text{O III}] \lambda 4959, 5007$ flux is just a few percent of the $\text{H}\beta$ line flux, and the corresponding value of $\log R_{23}$ is in the range -0.42 to -0.67 . Because of the rather flat relationship between O/H and R_{23} at

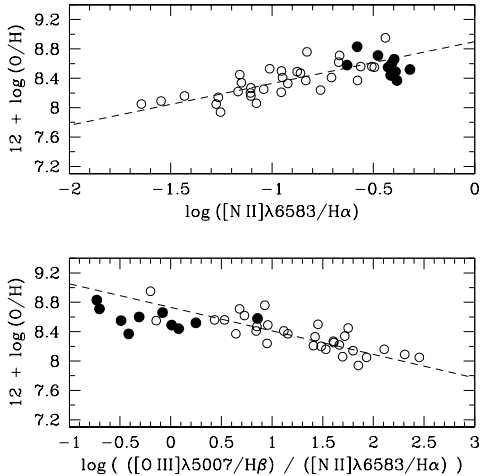


FIG. 8.— *Top*: O/H abundances obtained with the direct method are plotted against the line ratio $[\text{N II}]\lambda 6583/\text{H}\alpha$. Data are from this work (full dots) and from Kennicutt et al. (2003), Garnett et al. (1997) and Castellanos et al. (2002) (open circles). The dashed line is the regression taken from Pettini & Pagel (2004), obtained from a fit to a larger sample of H II regions. *Bottom*: Same as above, for the $([\text{O III}]\lambda 5007/\text{H}\beta)/([\text{N II}]\lambda 6583/\text{H}\alpha)$ index.

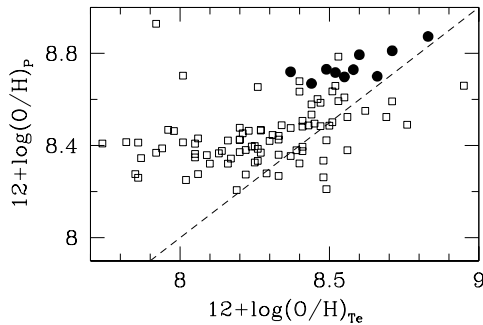


FIG. 9.— Comparison between direct O/H abundances and those obtained through the P-method of Pilyugin (2001). The data are from the current work (full dots) and from Kennicutt et al. (2003), Garnett et al. (1997), van Zee et al. (1998), Deharveng et al. (2000), Díaz & Pérez-Montero (2000) and Castellanos et al. (2002) (open squares). Only objects which are predicted by the P-method to have $12 + \log(\text{O}/\text{H}) > 8.2$ are plotted.

low excitation suggested by the M51 points in Fig. 7, these very low R_{23} values might still correspond to metallicities not much higher than solar [$12 + \log(\text{O}/\text{H}) \approx 8.8$ – 8.9], however any extrapolation to determine an oxygen abundance is at present still very uncertain. The dashed line in Fig. 7 shows such an extrapolation, determined from the M51 H II regions. The highest oxygen abundance in our sample, corresponding to $\log R_{23} = -0.66$ (the value for CCM 6A, CCM 37A and CCM 107 within ± 0.01), would be $12 + \log(\text{O}/\text{H}) \approx 8.86$ (1.5 times the solar O/H), comparable to our measured oxygen abundance for P 203.

We have estimated upper limits for the $[\text{N II}]\lambda 5755$ line in the spectra of the central objects. The results, summarized in Table 6, are not very compelling, and they are still consistent with abundances in the central region of M51 around the value found for P 203.

We finally point out that the $\text{He I}\lambda 5876/\text{H}\beta$ line ratio correlates with both O/H (for the objects in Table 1) and galactocentric distance (objects in Tables 1 and 6), as shown in Fig. 10. Together with the reduced excitation measured from the $[\text{O III}]\lambda 5007/\text{H}\beta$ ratio mentioned above, Fig. 10 shows how the ionizing field becomes softer towards higher metallicities, above a certain abundance threshold (the $\text{He I}\lambda 5876/\text{H}\beta$ ratio decreases below its saturation level, at which He is completely singly ionized, for $12 + \log(\text{O}/\text{H}) \geq 8.5$, top panel) and towards the galactic central regions (lower panel). The observed increase of the neutral helium fraction towards the metal-rich central region of M51 can be viewed as the result of the decrease in the equivalent effective temperature of the ionizing radiation field with increasing metallicity (see also Bresolin & Kennicutt 2002).

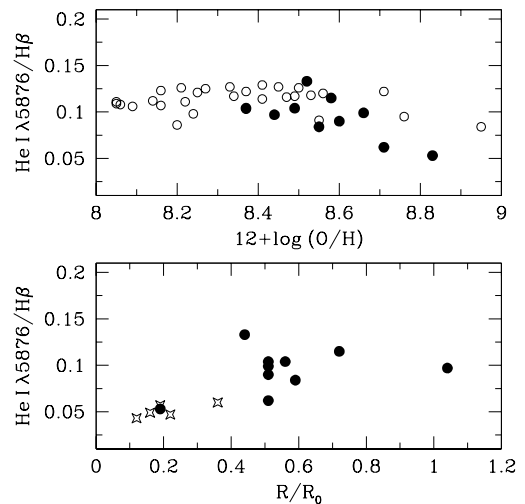


FIG. 10.— *Top*: A trend of decreasing $\text{He I}\lambda 5876/\text{H}\beta$ line ratio with abundance above $12 + \log(\text{O}/\text{H}) \approx 8.5$ is suggested here. The $\lambda 5876$ line has been corrected for an underlying absorption equivalent width of 0.8 \AA . Objects plotted are from M51 (filled dots) and M101 (open circles). *Bottom*: Variation of $\text{He I}\lambda 5876/\text{H}\beta$ with galactocentric distance for M51 H II regions. The filled dots are objects with a direct abundance determination, the open stars are objects of low excitation found in the central region of the galaxy.

6. WOLF-RAYET STARS

The main spectroscopic signature of WR stars (the blue bump at 4660 \AA) has been detected in six of the H II regions examined in this work. As shown in Fig. 11 we can clearly distinguish the stellar $\text{N III}\lambda 4634$ – 41 and $\text{He II}\lambda 4686$ lines in all cases, together with $\text{C IV}\lambda 4658$. Given the absence of $\text{N V}\lambda 4603$ – 20 , the morphology of the blue bump is characteristic of late WR subtypes (WNL). In addition, the $\text{C III}\lambda 5696$ line from WC subtype stars has been clearly detected in the two most metal-rich H II regions, CCM 72 and P 203. WR features have been detected in other M51 H II regions not analyzed in this paper. In CCM 13, 24, 41, 84A and 91 only the blue bump is present in our spectra. Both the 4660 \AA and

TABLE 6
LINE FLUXES OF LOW-EXCITATION OBJECTS

ID	R/R_0	$C(H\beta)$	$EW(H\beta)$ (Å)	[O II] 3727	[O III] 4959+5007	He I 5876	[N II] 6548+6584	[S II] 6717+6731	T[N II] (upper limit)	$12 + \log(O/H)$ (lower limit)
CCM 6A	0.12	0.10	55	17 ± 1	4.4 ± 0.3	3.9 ± 0.3	80 ± 4	26 ± 1	5800 K	8.40
CCM 37A	0.16	0.09	12	17 ± 1	4.8 ± 0.4	3.0 ± 0.3	54 ± 3	20 ± 1	6200 K	8.20
CCM 45	0.36	0.17	54	34 ± 2	4.2 ± 0.4	5.5 ± 0.5	116 ± 6	50 ± 3	5900 K	8.52
CCM 56	0.22	0.23	50	28 ± 2	8.5 ± 0.9	4.5 ± 0.5	121 ± 7	50 ± 3	5900 K	8.58
CCM 107	0.19	0.53	48	20 ± 1	2.6 ± 0.2	5.2 ± 0.3	98 ± 5	30 ± 2	5300 K	8.86

the 5696 Å features are seen in CCM 37A, 84 and 107, while only the 5696 Å line is visible in CCM 6A and 71 (also with 5810 Å). A marginal detection of He II λ 4686 has been made in a few additional objects, as well. Note that all the nebulae (except CCM 71) where the C III λ 5696 line has been detected are located at small galactocentric radii, or have a large O/H abundance (CCM 72). This agrees with the known trend of increasing fraction of WC relative to WN stars with abundance (Massey 2003).

The number of WNL stars can be estimated from the total He II λ 4686 line luminosity, assuming a fixed stellar luminosity of 1.6×10^{36} erg s⁻¹ (Schaerer & Vacca 1998). At the adopted distance to M51 of 8.4 Mpc the two objects with the highest He II luminosity (CCM 10 and CCM 72) are then found to contain five-six WNL stars each. The luminosity of the remaining objects is consistent with just one or two WNL stars being present. These numbers are not particularly remarkable when compared, for example, with the very large population of WR stars discovered by Crowther et al. (2004) in H II regions of another supposedly metal-rich galaxy, M83. Reporting the detection of WR features in solar-like abundance environments, however, is still of considerable interest, because of the trends one can establish between WR star population properties (e.g. their subtype distribution) and metallicity. It is also relevant to point out that WR features are found in very cool nebulae, such as the metal-rich CCM 72 and P 203, in support of the idea that the presence of these evolved massive stars does not significantly affect the ionizing properties of the embedded star clusters (Bresolin & Kennicutt 2002).

7. GAS FRACTIONS, EFFECTIVE YIELDS, AND CHEMICAL EVOLUTION

A comparison of observed abundances and gas fractions in galaxies provides interesting information on the effect of gas flows on galaxy evolution. Variations of the effective yield, defined as

$$y_{\text{eff}} = \frac{Z}{\ln(\mu^{-1})}, \quad (5)$$

where Z is the metallicity and μ is the gas mass fraction, are sensitive to gas inflow and outflow (Edmunds 1990; Köppen & Edmunds 1999). Garnett (2002) compared effective yields, derived from global abundance, stellar mass, and gas mass properties, in a sample of 50 nearby spiral and irregular galaxies, and found that y_{eff} varies systematically with galaxy rotation speed (and thus presumably total mass). The adopted interpretation was the low-mass irregular galaxies, with smaller effective yields than those derived for massive

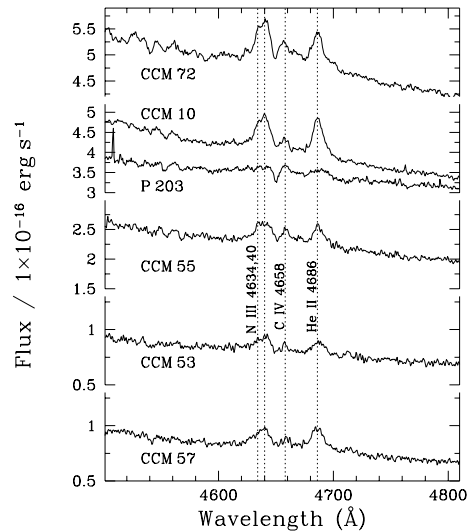


FIG. 11.— The WR stellar lines around 4660 Å have been detected in these six H II regions out of the ten analyzed. Feature identification is provided by the vertical dotted lines.

spirals, were losing a large fraction of their metals to the intergalactic medium (IGM).

Based on our new abundances for M51, we can re-evaluate its effective yield. Garnett (2002) used the measured abundance at one effective disk radius as a measure of the average metallicity of a spiral disk. From his Table 4, the adopted average $12 + \log(O/H)$ was 9.12 for M51. Our new value for $12 + \log(O/H)$ at $R_{\text{eff}} = 0.6 R_0$ is 8.55, a factor of 3.7 smaller. Thus the new value of y_{eff} we would derive is smaller by the same amount. Garnett (2002) derived $y_{\text{eff}} = 0.012$ for M51, so we would obtain $y_{\text{eff}} = 0.0032$ from our new data. This lower value is comparable to the values derived for smaller irregular galaxies such as IC 10 and NGC 6822 in Garnett's sample. Note also that this value of y_{eff} is much closer to that expected from stellar nucleosynthesis, and to the value obtained from estimates of the mean metallicity and gas fraction in the solar neighborhood. If other spirals show similar reductions in y_{eff} when more temperature-based abundance measurements become available, it may be necessary to re-examine the conclusions of Garnett (2002) regarding what galaxies may experience significant loss of metals.

It is also interesting and important to look at the variation of y_{eff} across a disk galaxy, to see if gas flows may play a role in the chemical evolution within the disk. A comparison between gas fraction and abundance across the disk has been done for only a few spirals to date.

We obtained the radial distribution of gas surface densities in M51 from the single-dish CO mapping of Kuno et al. (1995), measured with a $16''$ beam, and from the H I 21-cm map of Tilanus & Allen (1991). Young et al. (1995) also measured the radial distribution of CO, but their much larger beam size means that the mass surface density is averaged over a much larger area. We choose not to use measurements based on interferometers (e.g. Aalto et al. 1999), as they can miss significant amounts of extended emission due to missing short antenna baselines; we note that the measurements of Aalto et al. (1999) show a very sharply peaked CO flux distribution in rough agreement with Kuno et al. (1995). The derived molecular gas surface densities depend critically on the conversion from CO intensity to H_2 column density. We derived molecular surface densities under two assumptions for the $I(\text{CO})\text{-}N(\text{H}_2)$ conversion factor: (1) the ‘standard’ factor $3.0 \times 10^{20} \text{ cm}^{-2} (\text{K km s}^{-1})^{-1}$ (Wilson 1995), which includes a contribution for helium; (2) the smaller factor $1.3 \times 10^{20} \text{ cm}^{-2} (\text{K km s}^{-1})^{-1}$ used by Kuno et al. (1995) (adjusted here to include helium). Whichever value is used, the mass of molecular gas in M51 is quite large, and the mass surface density of H_2 exceeds that of atomic gas over much of the disk. The CO measurements do not go beyond $180''$ from the nucleus, so we have smoothly extrapolated the H_2 surface densities to larger radii based on an approximate exponential fit to the inner disk profile. Gas surface density distributions for a subset of our assumptions are shown in Figure 12.

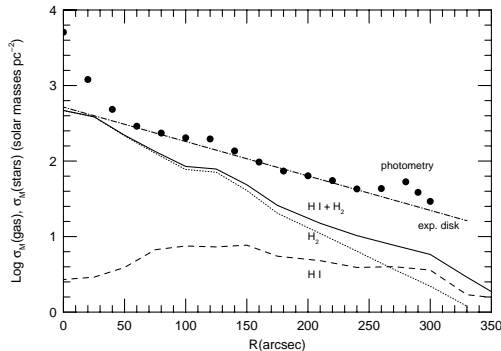


FIG. 12.— Gas and stellar mass surface density distributions in M51. The dashed line shows the H I surface density (adjusted for the presence of helium) from the data of Tilanus & Allen (1991). The dotted line shows the molecular gas profile obtained from the CO measurements of Kuno et al. (1995), assuming a CO- H_2 conversion factor of $3 \times 10^{20} \text{ cm}^{-2} (\text{K km s}^{-1})^{-1}$. The dot-dash line shows the mass profile for the stellar exponential disk determined as discussed in the text. The filled circles show stellar mass densities derived directly from the surface brightness data of Kuchinski et al. (2000).

The mass surface density for stars in M51 was derived from the BVRI surface photometry of Kuchinski et al. (2000). We converted the I-band surface brightnesses to mass surface densities by estimating the mass-to-light ratio (M/L) from the relations between M/L and color derived from stellar population models in Bell & de Jong (2001). From the Kuchinski et al. surface brightnesses, we estimated a central I-band disk surface brightness of $19.05 \text{ mag arcsec}^{-2}$ and a disk scale length of $114''$; we adopted a linear color profile with radius ranging from $B-R = 1.2$ at the center to $B-R = 0.9$ at $300''$. The resulting stellar mass profile for the disk in M51 is shown in Figure 12 as the dot-dash line, while the mass densities estimated directly from the photometry are shown as the filled

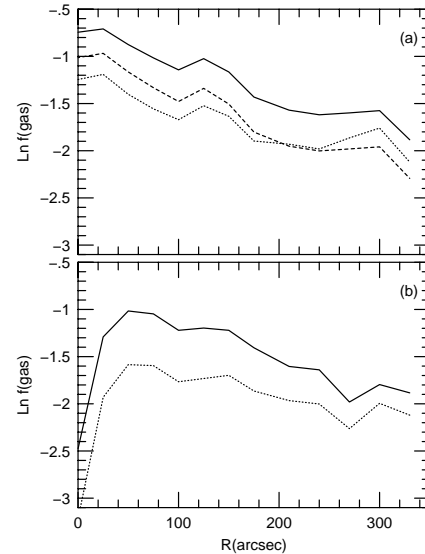


FIG. 13.— (a) The radial variation of the gas mass fraction for three different assumptions. *Solid line*: molecular gas masses estimated using $I(\text{CO})\text{-}N(\text{H}_2)$ conversion of 3.0×10^{20} ; *dashed line*: molecular gas mass densities estimated using $I(\text{CO})\text{-}N(\text{H}_2)$ conversion of 1.3×10^{20} ; *dotted line*: same gas densities as for solid line, but with stellar surface brightnesses adjusted for extinction $A(I) = 0.5 \text{ mag}$. (b) Radial variation of the gas fraction, where the stellar mass densities were derived directly from the I-band photometry, rather than the underlying exponential disk. *Solid line*: molecular gas densities obtained using $I(\text{CO})\text{-}N(\text{H}_2) = 3.0 \times 10^{20}$; *dotted line*: molecular gas densities obtained using $I(\text{CO})\text{-}N(\text{H}_2) = 1.3 \times 10^{20}$.

circles. Note that the photometry shows evidence for a central spheroidal component.

Inspection of Figure 12 shows one curious feature: the gas surface density profile is steeper than the stellar disk profile. This implies that the gas fraction decreases radially outward. We illustrate this in Figure 13(a), which shows the radial variation in three different cases: (1) $I(\text{CO})\text{-}N(\text{H}_2) = 3.0 \times 10^{20}$ (solid line); (2) $I(\text{CO})\text{-}N(\text{H}_2) = 1.3 \times 10^{20}$ (dashed line); and (3) a case similar to (1), but in which the stellar surface brightnesses have been adjusted upward for an extinction $A(I) = 0.5 \text{ mag}$ (dotted curve). In all three cases, the derived gas fraction declines by a factor 3-4 radially outward. This behavior contrasts strongly with that seen in other spiral galaxies, where the gas fraction increases outward (M81 - Garnett & Shields 1987; NGC 4254 - Henry et al. 1994; NGC 2403 and M33 - Garnett et al. 1997).

We have also looked at what happens if we simply use the observed surface brightness profile to derive the stellar mass densities, rather than an underlying exponential disk. The resulting gas profiles are shown in Figure 13(b), for our two assumptions of the $I(\text{CO})\text{-}N(\text{H}_2)$ conversion. While the resulting gas fractions for the inner disk are certainly smaller, due to the high central surface brightness, we still see a declining gas fraction with radius for $R > 50''$.

We note that a radial variation of a factor three in the CO- H_2 conversion is not sufficient to mitigate the decline in gas fraction. A factor six change in the conversion factor would be needed to flatten the gas fraction profile; such a variation is not at all predicted even by the most extreme estimates of metallicity variation in the conversion factor (Israel 1997). A

radial decline of about 1.5 mag in A(I) from the center to the outer disk would also be enough to flatten the gas fraction profile. Scoville et al. (2001) found a rough radial variation in A(V) for H II regions in the disk of M51, from $A(V) \approx 4$ in the inner disk to $A(V) \approx 2$ at $R = 300''$; however, it is not clear how to relate the extinction for H II regions, which are associated with gas and dust, to the extinction for the stellar disk. We also note that $A(I) = 0.5$ corresponds to $E(B-V) = 0.3$; with an observed $B-V$ of 0.6, such a correction for reddening would make M51 a very blue galaxy unless the reddening is very gray.

A radially decreasing gas fraction combined with a radially decreasing metallicity implies an effective yield that increases with metallicity. Such a variation was inferred by Vila-Costas & Edmunds (1992), but with older abundance data derived mainly from strong emission line calibrations. On the other hand, galaxies with abundances based on electron temperatures show little evidence for variations in effective yields (Garnett et al. 1997).

The peculiar gas fraction profile in M51 may also point to dynamical influences. M51 is an interacting system. Fly-by interactions of this type can lead to bar formation, which induces radial flows of gas toward the center of the galaxy. Pierce (1986), Kohno et al. (1996), and Aalto et al. (1999) have presented photometric and kinematic evidence for a bar in the central regions of NGC 5194, while infrared imaging reveals that NGC 5195 has an obvious bar (e.g., the I-band images of Kuchinski et al. 2000). It is possible that the interaction and bar have driven gas into the central regions of M51, leading to the very steep gas profile we see. This would complicate the interpretation of the chemical evolution of this system, and requires dynamical and photometric modeling that is beyond the scope of this work.

8. CONCLUSIONS

We have analyzed a sample of ten H II regions in the spiral galaxy M51 where at least one of the auroral lines [N II] $\lambda 5755$ and [S III] $\lambda 6312$ could be measured, and we discussed the resulting oxygen, sulfur and nitrogen abundances. The single, most remarkable result obtained is that in M51 the direct O/H abundances are considerably below the value obtained either from photoionization models (Díaz et al. 1991) or from empirical abundance indicators. The calibration of the latter depended so far, in the low-excitation range defined mostly by H II regions in M51, on the abundances obtained

from the models, therefore the two are not independent. We have not attempted to generate improved nebular models, for example including more recent stellar atmospheres for the treatment of stellar ionizing fluxes. This aspect needs to be explored in the future.

The result concerning O/H has important implications for the calibration of empirical abundance indicators, and in general for the determination of abundance gradients in spiral galaxies. Our result, combined with previous ones obtained for smaller samples of metal-rich H II regions by Castellanos et al. (2002), Díaz et al. (2000) and Kennicutt et al. (2003), points to shallower gradients. H II regions once believed to have O/H abundances equal to 2–3 times solar are found by the direct method to rarely exceed the solar value, and if so by a moderate amount, up to 50 percent.

Our analysis has also established that in our M51 sample the abundance ratio S/O is similar to the value found at lower O/H abundance in other spiral galaxies. We find no evidence for a decrease in S/O with increasing O/H, which would occur in case of a differing initial mass function and/or nucleosynthesis for massive stars. The nitrogen abundance has a mean value $\log(N/O) \simeq -0.6$, larger than in later spirals like M101, but this can still be interpreted with the known spread of N/O at a given oxygen abundance.

The lower oxygen abundance we measure in M51 with respect to previous determinations has also allowed us to revise the effective yield of this galaxy. From a rather peculiar gas fraction radial profile we infer an effective yield increasing with metallicity.

The number of galaxies with reliable *direct* measurements of nebular chemical abundances extending over their whole disks, including the metal-rich central zones, is still very limited. These measurements are necessary for the correct determination of the chemical compositions in galactic disks and their interpretation in terms of chemical evolution models. The current work on M51 demonstrates that large samples of metal-rich H II regions can be efficiently studied in spiral galaxies with current telescopes and instrumentation.

We thank T. Rector for the Kitt Peak 0.9m H α image of M51 used for Fig. 1. RCK acknowledges NSF grant AST-0307386 and NASA grant NAG5-8426. DRG acknowledges NSF grant AST-0203905 and NASA grant NAG5-7734.

REFERENCES

- Aalto, S., Hüttemeister, S., Scoville, N. Z., & Thaddeus, P. 1999, *ApJ*, 522, 165
 Allende Prieto, C., Lambert, D.L., & Asplund, M. 2001, *ApJ*, 556, L63
 Alloin, D., Collin-Soufrin, S., Joly, M., & Vigroux, L. 1979, *A&A*, 78, 200
 Bell, E. F., & de Jong, R. S. 2001, *ApJ*, 550, 212
 Bresolin, F., & Kennicutt, R.C. 2002, *ApJ*, 572, 838
 Bresolin, F., Kennicutt, R.C., & Garnett, D.R. 1999, *ApJ*, 510, 104
 Cardelli, J.A., Clayton, G.C., & Mathis, J.S. 1989, *ApJ*, 345, 245
 Carranza, G., Crillon, R., & Monnet, G. 1969, *A&A*, 1, 479
 Castellanos, M., Díaz, A.I., & Terlevich, E. 2002, *MNRAS*, 329, 315
 Crowther, P.A., Hadfield, L.J., Schild, H., & Schmutz, W. 2004, *A&A*, in press
 Deharveng, L., Peña, M., Caplan, J., & Costero, R. 2000, *MNRAS*, 311, 329
 Denicoló, G., Terlevich, R., & Terlevich, E. 2002, *MNRAS*, 330, 69
 Díaz, A. I., Castellanos, M., Terlevich, E., & García-Vargas, M.L. 2000, *MNRAS*, 318, 462
 Díaz, A. I., & Pérez-Montero, E. 2000, *MNRAS*, 312, 130
 Díaz, A.I., Terlevich, E., Vílchez, J.M., Pagel, B.E.J., & Edmunds, M.G. 1991, *MNRAS*, 253, 245
 Dopita, M.A., & Evans, I.N. 1986, *ApJ*, 307, 431
 Edmunds, M. G., 1990, *MNRAS*, 246, 678
 Edmunds, M.G., & Pagel, B.E.J. 1984, *MNRAS*, 211, 507
 Feldmeier, J.J., Ciardullo, R., & Jacoby, G.H. 1997, *ApJ*, 479, 231
 French, H.B. 1981, *ApJ*, 248, 468
 Garnett, D.R., Kennicutt, R.C., & Bresolin, F. 2004, *ApJ*, in press
 Garnett, D.R. 2004, in *Cosmochemistry: The Melting Pot of the Elements. XIII Canary Islands Winter School of Astrophysics*, ed. by C. Esteban, R.J. García Lopez, A. Herrero & F. Sanchez (Cambridge: CUP), p. 171
 Garnett, D. R. 2002, *ApJ*, 581, 1019
 Garnett, D.R., Shields, G.A., Skillman, E.D., Sagan, S.P., & Dufour, R.J. 1997, *ApJ*, 489, 63
 Garnett, D.R. 1992, *AJ*, 103, 1330
 Garnett, D. R., & Shields, G. A. 1987, *ApJ*, 317, 82
 Henry, R. B. C., Edmunds, M. G., & Köppen, J. 2000, *ApJ*, 541, 660
 Henry, R. B. C., Pagel, B. E. J., & Chincarini, G. 1994, *MNRAS*, 266, 421
 Israel, F. P., 1997, *A&A*, 328, 471
 Izotov, Y.I., Thuan, T.X., & Lipoyetsky, V.A. 1994, *ApJ*, 435, 647
 Kennicutt, R.C., Bresolin, F., & Garnett, D.R. 2003, *ApJ*, 591, 801
 Kewley, L.J., & Dopita, M.A. 2002, *ApJS*, 142, 35
 Kinkel, U., & Rosa, M.R. 1994, *A&A*, 282, L37

- Kobulnicky, H.A., Henry, A., & Phillips, A.C. 2003, *ApJ*, 599, 1031
Kohno, K., Kawabe, R., Tosaki, T., & Okamura, S. K., 1996, *ApJ*, 461, L29
Köppen, J., & Edmunds, M. G., 1999, *MNRAS*, 306, 317
Krisciunas, K., Sinton, W., Tholen, K., Tokunaga, A., Golisch, W., Griep, D., Kaminski, C., Impey, C., & Christian, C. 1987, *PASP*, 99, 887
Kuchinski, L. E., et al. 2000, *ApJS*, 131, 441
Kuno, N., Nakai, N., Handa, T., & Sofue, Y., 1995, *PASJ*, 47, 745
Liu, X.-W., Storey, P.J., Barlow, M.J., Danziger, I.J., Cohen, M., & Bryce, M., 2000, *MNRAS*, 312, 585
Massey, P. 2003, *ARAA*, 41, 15
McGaugh, S.S. 1991, *ApJ*, 380, 140
Oke, J.B., Cohen, J.G., Carr, M., Cromer, J., Dingizian, A., Harris, F.H., Labrecque, S., Lucinio, R., Schall, W., Epps H., and Miller, J. 1995, *PASP*, 107, 375
Pagel, B.E.J., Edmunds, M.G., Blackwell, D.E., Chun, M.S., & Smith, G. 1979, *MNRAS*, 189, 95
Petit, H., Hua, C.T., Bersier, D., & Courtès, G. 1996, *A&A*, 309, 446
Pettini, M., & Pagel, B.E.J. 2004, *MNRAS*, 348, 59
Pierce, M. J., 1986, *AJ*, 92, 285
Pilyugin, L.S., Thuan, T.X., & Vílchez, J.M. 2003, *A&A*, 397, 487
Pilyugin, L.S. 2001, *A&A*, 369, 594
Pilyugin, L.S. 2000, *A&A*, 362, 325
Schaerer, D., & Vacca, W.D. 1998, *ApJ*, 497, 618
Scoville, N. Z., Polletta, M., Ewald, S., Stolovy, S. R., Thompson, R. I., & Rieke, M., 2001, *AJ*, 122, 3017
Shaw, R.A., & Dufour, R.J. 1995, *PASP*, 107, 896
Stasinska, G., Schaerer, D., & Leitherer, C. 2001, *A&A*, 370, 1
Stasinska, G. 1990, *A&AS*, 83, 501
Stasinska, G. 1978, *A&A*, 66, 257
Tayal, S.S., & Gupta, G.P. 1999, *ApJ*, 526, 544
Tilanus, R. P. J., & Allen, R. J. 1991, *A&A*, 244, 8
van Zee, L., Salzer, J.J., Haynes, M.P., O'Donoghue, A.A., & Balonek, T.J. 1998, *AJ*, 116, 2805
Vila-Costas, M.B., & Edmunds, M.G. 1992, *MNRAS*, 259, 121
Vílchez, J.M., & Pagel, B.E.J. 1988, *MNRAS*, 231, 257
Young, J. S., et al. 1995, *ApJS*, 98, 219
Wilson, C.D. 1995, *ApJ*, 448, L97
Zaritsky, D., Kennicutt, R.C., & Huchra, J.P. 1994, *ApJ*, 420, 87